Talanta 128 (2014) 414–421

Contents lists available at ScienceDirect

Talanta

journal homepage: www.elsevier.com/locate/talanta

Evanescent-field-induced Raman scattering for bio-friendly fingerprinting at sub-cellular dimension

Boris Snopok [a,b,e,*], Denys Naumenko [a], Elena Serviene [c,d], Ingrida Bruzaite [c], Andrius Stogrin [a], Juozas Kulys [b,c], Valentinas Snitka [a]

[a] Kaunas University of Technology, Research Centre for Microsystems and Nanotechnology, Studentu 65, 51369 Kaunas, Lithuania
[b] Vilnius University, Institute of Biochemistry, Mokslininkų 12, 08662 Vilnius, Lithuania
[c] Vilnius Gediminas Technical University, Department of Chemistry and Bioengineering, Sauletekio al. 11, LT-10223 Vilnius, Lithuania
[d] Nature Research Centre, Akademijos 2, 08412 Vilnius, Lithuania
[e] V. Ye. Lashkaryov Institute of Semiconductor Physics, National Academy of Sciences of Ukraine, Prospekt Nauky, 41, Kyiv 03028, Ukraine

ARTICLE INFO

Article history:
Received 24 January 2014
Received in revised form
2 April 2014
Accepted 5 April 2014
Available online 26 April 2014

Keywords:
Evanescent wave
Surface plasmon resonance
Raman scattering
Tip enhanced Raman spectroscopy
μ–TERS
Yeast cell
Cellular envelope
Atomic force microscopy
Dried biological samples

ABSTRACT

Evanescent field induced chemical imaging concept has been realized in analytical platform based on the μ-tip-enhanced Raman scattering spectroscopy (μ-TERS). The technique aimed to minimize thermal decomposition of dried biological sample as the result of huge concentration of optical field near the tip by increasing the size of an aperture-less "excitation source". μ-TERS technique is similar to classical biosensor systems based on propagating surface plasmon resonance phenomenon but with sensitive elements a few micrometers in size that can be targeted to the area of interest. The utility of the concept is exemplified by the analysis of dried single cell envelope of genetically modified *Saccharomyces cerevisiae* yeast cells, which do not have any heat-removing pathways, by water as in the case of the living cell. Practical excitation conditions effective for μ-TERS Raman observation of single layer dried biological samples without photodamage-related spectral distortion have been determined – the allowable limit is above 30 s at 13 $\mu W/\mu m^2$. Finally, potential of μ-TERS spectroscopy as new bio-friendly instrumental platform for chemical fingerprinting and analytical characterization of buried nanoscale features is discussed.

1. Introduction

Local optical identification of biological structures is of fundamental importance to reveal the details of animate nature exploring the physical properties of matter for functional visualization [1,2]. To characterize molecular interactions and signal transduction pathways at sub-cellular dimension – the ultimate limit in cell biology – new sensing strategies are requested [3]. The key feature of such approaches relies on the dimension of the physical transducer being similar to the sub-structures they are sensing. Because cells typically range in tens of micrometers with functional sub-structures in the range of tens-hundreds of nanometers in size, it is challenging to (i) identify the region of specific supramolecular machine and (ii) relocate the probe into the place of interest. In the case of label free technologies it can be done if the sample and physical transducer are spatially separated enabling chemical characterization of extended biological object by scanning protocols; final positioning of the transducer within definite area of the sample may be realized using specific fingerprint of a target component (Fig. 1).

Classical near-field analytical systems based on aperture-based scanning optical microscopy [4] or supercritical angle fluorescence spectroscopies [5] etc. are typical but expensive examples of such approaches. Raman spectroscopy has also emerged as useful techniques, which can afford rich chemical information using visible light in both water and air environments and characterize complex supramolecular architectures by vibrational fingerprint (virtual chemical image) [6–9]. In particular, the Raman-based non-destructive chemical imaging resolves the functional structures with the microscale resolution and their changes during biochemical processes in real time [10–12].

Local spatial targeting of the Raman effect was realized in tip-enhanced Raman spectroscopy (TERS) by combination of vibrating spectroscopy and scanning probe microscopy (SPM) [13] in the aperture-less optical setup with ultrahigh spatial resolution. To obtain requested spatial resolution TERS uses strongly localized field enhancement, where this enhanced interaction volume acts as an excitation source with the size similar to the objects under investigation. Contrary to the stable and high efficient Raman scattering materials [14–16] for biological objects Raman scattering is week, so

* Corresponding author at: Kaunas University of Technology, Research Centre for Microsystems and Nanotechnology, Studentu 65, 51369, Kaunas, Lithuania.

http://dx.doi.org/10.1016/j.talanta.2014.04.015
0039-9140/

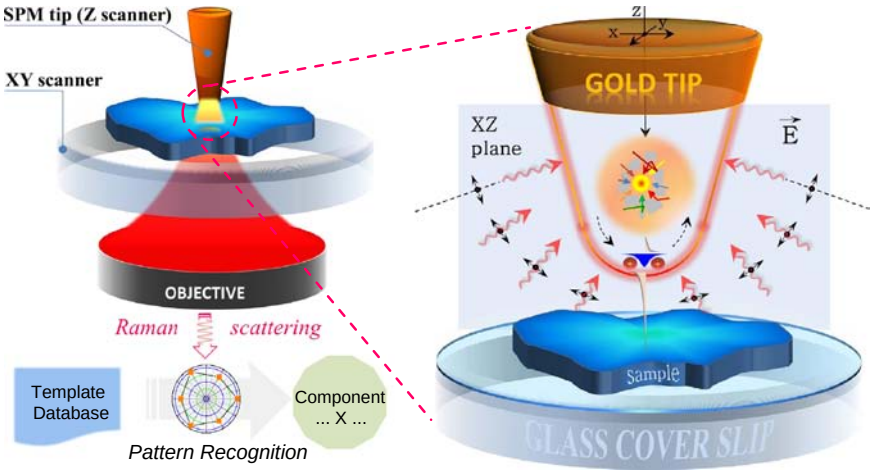

Fig. 1. Schematic diagram of core processes is illustrating the concept of biosensing platform for evanescent field induced chemical imaging (left) and the generation and propagation of surface plasmon polaritons at the surface of the perispheric submicron tips in the focal plane of the objective with high numerical aperture lens (right).

for the reasonable signal-to-noise level long acquisition time or high laser intensity are necessary, which may destroy the biological samples. Indeed, owing to high thermal instability of (bio)organic molecules many of them under the TERS conditions reduce to so-called "carbon contamination" as a result of thermal decomposition (burning) [17,18] or "synthesis" of new compounds by plasmon-driven chemical reactions [19]. So, in the case of bio-optical characterization it is necessary to find such a level of optical field concentration that can be acceptable for adequate functioning of molecular biosystems from one side and will be strong enough for detection of Raman effect that – as an inelastic scattering process – is week.

Spatial confinement of light can be implemented in a variety of ways using effects of propagating or localized surface plasmon resonance phenomena. For the metal SPM tip a typical way to concentrate optical energy is to confine light in the form of evanescent wave using plasmonic taper or metal nanoparticles [20,21]. In the classical nano-focusing tapered structures with the sharp tips (~5–20 nm) significant accumulation of optical energy is the result of excitation of propagating surface plasmon polaritones (SPP) that are slowed down and adiabatically stopped at the apex depositing a significant fraction of their energy to the tip [22,23]. Adiabatic nano-focusing is strongly dependent on the radius of the tip, with significant field enhancement observed only at sharp tips, whereas the SPP propagation along the curved metal surface whose diameters are about the light wavelength or bigger seem similar the situation on the flat metal surface [24]. In this case the electromagnetic energy is compressed in the area occupied by the evanescent wave in the dielectric and even for the flat surface may essentially enhance the Raman scattering [25,26,16]. In the present work we discuss new abilities of the concept based on a combination of classical TERS approach and conventional SPR based biosensors, namely, tip enhanced Raman scattering technique with high radius tips (μ-TERS) for adequate analysis of ultrathin dried biological samples. In some sense μ-TERS is similar to classical biosensor systems based on propagating surface plasmon resonance phenomenon but with sensitive elements a few micrometers in size that can be targeted to the area of interest. Results of numerous studies validate the correctness of long-time monitoring of biological samples under SPR conditions without essential loss of their biological function [27–30]. Moreover, we demonstrate that μ-tip enhanced optical readout can be efficiently used for chemical characterization of cell envelope of single living yeast cell without their damage during the measurements [31]. However, the TERS with micrometer tips is never used for remote probing of extracted, usually dried, biological materials which on the contrary to whole cell do not have any heat-removing water outflows.

In the present work we discuss the potential of the μ-tip-enhanced Raman scattering spectroscopy (μ-TERS) as a biologically friendly concept based on evanescent field induced chemical imaging for analysis of dried sub-cellular structures. The utility of the concept is exemplified by the analysis of single cell envelope of genetically modified *Saccharomyces cerevisiae* yeast cells, one of the most extensively studied model eukaryotic organisms.

The paper is organized as follows. It begins by discussing the methodological aspects of the μ-TERS spectroscopy as a biologically friendly technique suitable for analysis of buried or subsurface structures, a cell modification protocol, experimental setups, tips preparation etc. This is followed by the results of topographical imaging of yeast cell envelope by atomic force microscopy (AFM) and chemical characterization performed by μ-TERS. Finally, the potential of μ-TERS spectroscopy as an instrumental platform for chemical fingerprinting and analytical characterization is discussed.

2. μ-Tip-enhanced Raman spectroscopy for careful analysis of buried or subsurface structures

The classical TERS with a huge enhancement factor (often 10^7 or more) of the Raman scattering from an object near the sharp tip has an extremely small "excitation volume". As the result of huge concentration of optical field near the tip apex, signal instabilities in the form of signal losses and spectral fluctuations with time have been widely observed in TERS for the samples which are not so stable as carbon materials or laser dyes [17–19]. As an expressive example of the temperature gradients in the "hot" tip-sample nanogap is the local annealing of the Au surface by the Joule heating generated by the highly enhanced electromagnetic field [32]. To exclude possible thermal decomposition of the sample within the "hot" area one of the possible ways is the spreading of the less enhanced optical field to the bigger volume increasing the diameter of the tip apex and thereafter the size of an aperture-less "excitation source".

The amplification mechanism of optical field (with wavelength λ) for μ-TERS tips with micrometer range radius R differs significantly from the conventional tapered structures terminated by a sharp tip r – $r \ll \lambda$ and $R \geq \lambda$ for TERS and μ-TERS correspondingly [31,33,34]. With the increase of the tip radius intensity of electromagnetic field, the resolution and field enhancement at the tip apex are reducing, whilst the penetration depth of the evanescent wave is extended up to the order of the wavelength on a flat surface [24]. It is the result of the disturbing of the conditions required for realization of adiabatic nanofocusing mechanism in sharp tips or "SERS-specific" amplification mechanism in nanostructures when both incident and scattered

fields are in resonance with the electromagnetic excitations (localized surface plasmons) in "antenna"/"source" [35].

Similar to classical SPR-based biosensors [24,27–30], the large enough enhancement of local electromagnetic fields required for adequate optical detection of Raman scattering can be realized using spatial confinement of light near the surface in the form of evanescent wave of surface plasmon polaritones [24]. Due to the large radius of curvature of the probe termination, the SPP may propagate continuously along the tip surface with relatively low radiation loss without change of SPP wavelength. In this case the electromagnetic energy is compressed in the area occupied by the nonradiative evanescent wave around the tip resulting in accumulation of optical energy near the metal surface [36,37]. It should be mentioned though, that an exact theoretical solution of SPP focusing by tapered structures terminated by a perispheric submicron tip near the focus of high NA lens is still unknown.

Finally, it is reasonable to discuss some practical aspects of the μ-TERS techniques. First, plasmon states are the surface waves and for coupling between them external radiation vector of the light must be changed through diffraction on the rough tip surfaces [24]. SPP can be excited by p-polarized radiation (the electric vector $E^{\rightarrow}$ lies in the plane of incidence, Fig. 1), since an electric field with components directed along and normal to the metal surface is necessary for the generation of surface charge. The tangential component of the incident radiation must coincide with the wave vector of the SPP; so, in the case of rough tips the most efficient generation of SPP will occur at certain angles when the surface relief profile will ensure the generation of surface coupled excitations. In our experimental set-up the laser illuminates the tip in transmission mode through a high NA objective within a wide range of incident angles ($\pm 60^{\circ}$). As it is well known, in this backscattering or reflecting geometry, above and below the position of the actual focus, z-contribution of the field vectors can be found [32]; in line with that we used slightly unfocused laser beam whose focus has been shifting up in respect to the tip apex; it permits to generate optical field suitable for SPP excitation. More information concerning the optical field distribution near the focus of high NA lens can be found in [40–43].

A second essential feature of μ-TERS techniques is the presence of a strong nonuniform electric field whose intensity below the tip apex decays exponentially as $\exp(-d/\delta)$, where d is the distance from the tip [38]. Contrary to classical TERS the penetration depth of evanescent wave δ in a medium in contact with the metal lies in the range of hundreds of nanometers (*c.a.* $\delta \approx 0.37\lambda$ [24,39]) depending on the light wavelength λ and on the type of material. It has opened the way for analysis of buried or subsurface structures. The penetration depth of the evanescent wave outside the metal is roughly similar to that on a flat surface; however, the nonuniform character of evanescent wave must be taking into account for adequate analysis [24].

The third remarkable feature of the SPP is the possibility to propagate along the surface of the metal through distances that significantly exceed their wave length. As a result, surface waves propagate in various directions reflecting on steric hindrances, interact and decay (Fig. 1) by spreading along a rough surfaces. As a result, for the metal SPM tip with a spherical-like metal surface at the tip apex (whose sizes are about the light wavelength) polarization dependent geometrical focusing due to SPP annular propagation towards the tip of the hemisphere is well possible. Indeed, the distribution of electromagnetic field around a metal tip depends on the polarization direction of the incident laser. As seen from Fig. 1, in the case of linearly polarized light along x axis (at the sample plane) the surface charges within YZ plane is "spreaded" in the direction perpendicular to the direction of propagation and disturb the spatially localized system of charges required for the generation of stable plasmon–polariton excitation. The best excitation conditions realized for the case when electrical field lie within XZ plane (Fig. 1). So, the area of high electromagnetic field in the vicinity of the tip apex is ellipsoidal with long axis coincident with polarization direction and dimension that is essentially smaller in respect to the tip diameter. So, contrary to the high-resolution TERS with *maximum* scope restricted roughly [38,44] by $r \times r \times r$ (r is the tip radius in nanometer range), in the μ-TERS we can highlight the volume with $(\gamma R)(\mu R)\delta$ in size ($\delta \approx 0.37\lambda$, R in sub-micrometer range and $\gamma < 1$, $\mu \ll 1$).

3. Experimental section

3.1. Yeast cell growth, isolation of membrane fraction and GDH protein purification

The genetically modified *S. cerevisiae* yeast strain 21PMR-[pYEsec1-GDH] [31,45] was grown with aeration in the liquid YPG media (1% yeast extract, 2% peptone, 3% galactose) for 24 h at 30 °C. The presence of *Kluyveromyces lactis* toxin signal sequence in the genetic design of GDH assumes the secretion of the synthesized protein into the extracellular medium. The yeast cells were harvested by centrifugation (3000 g) at 4 °C for 10 min, resulted biomass (1 g) was resuspended in 2 ml of PBS buffer and ground using liquid nitrogen. The unbroken cell fraction was removed by centrifugation (1000*g*) at 4 °C for 5 min. Cytoplasmic fraction was cleared by centrifugation (11000*g*) at 4 °C for 15 min. The resting sediments (cell wall and membrane fraction) were twice-washed with PBS buffer and kept at 4 °C until used for spectroscopic analysis. GDH protein purification was described in [31]. The specific activity of GDH (U/ml) was determined in a crude yeast extract and in cytoplasmic or membrane fractions by measuring the decrease in DCIP absorbance at 600 nm. It was found that maximal GDH activity is in solubilized membrane protein fraction (~40 U/mL) compared to localized in cytoplasm (29 U/mL) or secreted form (trace amounts) [46].

3.2. Sample preparation and AFM imaging

Droplet of the PBS solution with dispersed cell envelope was dried at room temperature (20 ± 2 °C) on a clean glass microscope slide coverslips (24 × 24 × 0.15 mm^3, Carl Roth GmbH, Germany) without any additional coating. Samples were characterized by AFM (NTEGRA Spectra system, NT-MDT Inc., Russia) in the tapping mode using commercial silicon cantilevers NSG11 with a force constant of 5 N m^{-1} at a scan rate of typically 1 Hz.

3.3. Raman spectroscopy measurements

Raman spectra are measured using a confocal Raman system (NTEGRA Spectra, NT-MDT, Russia) that has been described previously [31]. The laser beam of 35-mW He-Ne laser (632.8 nm, Melles Griot 25-LHP-928-230, USA) is delivered through a clean-up filter into an inverted optical microscope (Nikon Eclipse TE 2000-S). The microscope is equipped with a 100 × 1.32 numerical aperture oil immersion objective (Leitz NPL Fluotar, Germany). In the present work we used partly unfocused laser beam with above 5 μm diameter and laser power of 1 mW (ca. 13 μW/μm^2) at the sample plane. The beam is focused through a glass cover slip, which is fixed on a controlled XY scanning stage (50 × 50 μm^2). 633- ultrasteep long-pass edge filters reject residual backscattered laser light and the signal is directed into a spectrometer (Solar TII, NT-MDT) equipped with a TE-cooled (−70 °C) CCD camera (DV401-BV, Andor Technology, USA). Using the additional Scanning Probe Microscopy platform (for shear-force mode with tuning fork piezoelectric linear actuator), the apex of gold tip was positioned within the focused beam on the measured sample.

In the present work the tips were produced by the electrochemical etching (10 V, 10 kHz, 10–30 s) of thin gold wire (99.99% pure gold wire of 125 μm in diameter, GoodFellow, Cambridge Limited, England) in a $CaCl_2$ saturated solution twice diluted with water [31]. Before etching, the gold wire was cleaned and glued to a quartz tuning fork transducer. The fabricated probes have an apex diameter in sub-micrometer range (typically 400–600 nm) and show a Q-factor value of above 500–700 at a resonant frequency of above 190 kHz.

3.4. Spectral Preprocessing

Following the spectral acquisition, the background spectrum was subtracted from each spectrum at first; then spectra were corrected from the fluorescence input by subtraction of fourth order polynomial curves (multipoint baseline) using both wavelet and moving average filters by Raman Processing Program [47,48].

The band specific experimental Raman enhancement factor G_s has been deduced from the increase in intensity within the specific Raman bands using

$$G_s = \frac{\int_{\delta_n-\Delta}^{\delta_n+\Delta} I(\delta)^{\mu-TERS}(\delta)\mathrm{d}\,\delta}{\int_{\delta_n-\Delta}^{\delta_n+\Delta} I(\delta)^{\mu-Raman}(\delta)\mathrm{d}\,\delta} \quad (1)$$

where $I(\delta)^{\mu\text{-}TERS}$ and $I(\delta)^{\mu\text{-}Raman}$ are the intensity of background/fluorescence corrected μ-TERS and μ-Raman responses respectively, δ is the Raman shift, δ_n is the position of n Raman band, and $\Delta = 15\ \mathrm{cm}^{-1}$ in the present case.

Changes in chemical images (vibrational fingerprints) of the samples were analyzed using polar diagrams similar to ones used in analysis of multichannel arrays [49,50]. The intensity of Raman based was normalized in line with the procedure

$$I(\delta_i) = \frac{\delta_i}{\sum_{i=1}^{n}\delta_i} \quad (2)$$

where δ_i is the Raman shift of i-band and n is the number of bands used for fingerprinting.

4. Results

4.1. AFM imaging of yeast cell envelope

The optical images of the dried cell envelopes on the glass substrate indicate the presence of multilayer aggregates and a few areas potentially covered by single layer flakes (Fig. 2). AFM imaging resolves the detailed structural features on the surface providing better visualization and allows separating the single layer areas. Fig. 2 shows typical AFM images taken from the dried single cell envelope on the glass. The thickness of the layer is *c.a.* 100 nm that is in good agreement with results of other authors [51]. High-resolution AFM imaging of the cell envelope of yeast shows some interfacial structures with lateral size in the range of 20–100 nm and 3–7 nm in height with homogeneous spatial distribution. It is reasonable to assume that observed elements of the surface profiles are the result of protein aggregates etc. located within the periplasm of cell envelope [31].

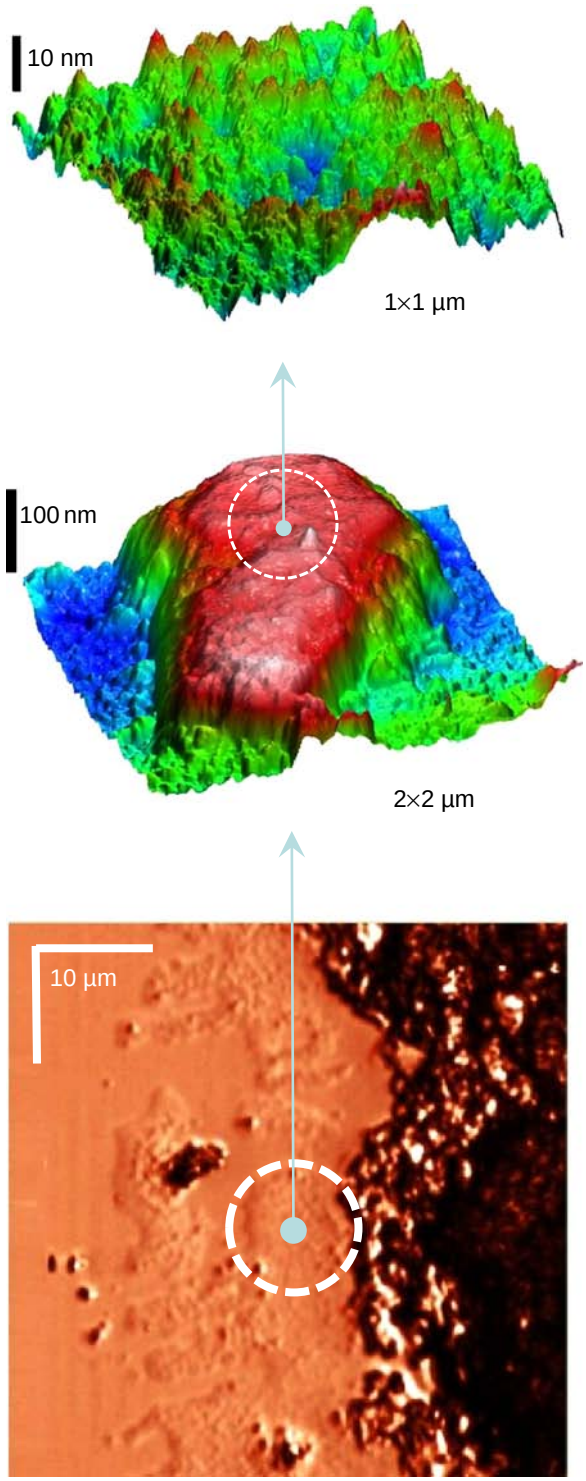

Fig. 2. Optical image (bottom) of dried yeast envelope solution containing both single and multilayer areas as well as AFM images of single cell envelope (middle) and topography of membrane surface (top). Thickness of single layer area is above 100–120 nm.

4.2. μ-Ters spectra of single cell envelope: tentative band assignment

The area on the glass surface with the single cell envelope revealed by AFM was used for Raman investigations. Fig. 3 shows the substrate corrected typical Raman spectra in the range of 900 to 1900 cm^{-1} registered by the consecutive measurements at the same point; spectra have been scaled to the same acquisition time (10 s). The μ-TERS spectra with different light durations (10, 40 (=10+30) and 100 (=10+30+60) s as the result of consequent measurements with acquisition time 10, 30 and 60 s) match each other well in the 800–1100 cm^{-1} region. The ratio of normalized and difference spectra presented in Fig. 4 confirms this conclusion. At the same time, there is some redistribution of Raman intensity in other areas: with increasing duration time, the intensity of the component with a Raman shift more than 1000 cm^{-1} decreases (Fig. 3), whereas at smaller than 1000 cm^{-1}, increases (data not shown).

First of all it is reasonable to note that observed enhancement of both fluorescence and Raman signals (the enhancement factor G_s is above 3.5–4.5, Fig. 3) cannot be explained by an additional reflection from the tip approaching the surface. The reasons for that are the conical form of the tip, its small size in respect to the laser beam and similar signal at glass surface for both tip-down and tip-up configurations.

Data presented in Fig. 3 indicate that the μ-Raman spectra cannot be used for the characterization of the sample due to the low quality of the data whereas in the μ-TERS spectra the characteristic peaks are clearly identified. It is important to note that although some specific assignment of Raman bands can be made, many of the changes are in spectral regions characterized by significant overlap between proteins, lipids and polysaccharide peaks. So, well-defined analysis with the molecular identification is difficult due to complex multicomponent composition of the cell envelope. Spectrum has prominent bands in the region between 900 and 1800 cm^{-1}, namely, 1004 (Proteins: Phe), 1145, 1215 (P: Phe, Tyr), 1280 (P: Amide III area), 1360–1390, 1440–1470 (C–H vibrations corresponding to all cellular components), 1560, 1605 (P, Lipids: C–C vibrations), 1640 (P: Amide I area) and 1725 (L: C=O stretch) cm^{-1}. Hence, spectrum corresponds more likely to lipids and proteins [12,52,53].

In the present study we used dried envelope fragments of genetically modified yeast cells enriched by GDH protein. It is difficult to correctly identify the GDH specific bands within the spectra of single layer envelope owing to relatively low concentration of GDH protein in the membrane fraction (less than 0.1%). However, at least it is possible to conclude that obtained spectra are in line with assumption of GDH proteins arrangement within the periplasm of prokaryotic cells confirmed by biochemical study [46] and supported by AFM imaging and Raman scattering [31,54,55].

4.3. *Photo-bleaching of Raman scattering and possible photodamage on single yeast cell envelope depending on duration of light exposure*

The intensity of the both fluorescence emission and Raman scattering are depending on duration of light exposure (Figs.3, 5). The quantitative analysis of the μ-TERS spectra of envelope obtained for different durations (10, 40, 100 s) of sample exposure shows that intensity of the Raman band specific for nonpolar phenylalanine amino acid (1004 cm^{-1}) do not fade essentially (Figs. 3–4). So, the baseline/fluorescence corrected spectra have been normalized to an intensity of a sharp band at 1004 cm^{-1} specific for the phenylalanine ring breathing vibrations (Fig. 5).

Spectra obtained from the sample with relatively short duration of light exposure (10–30 s at 13 μW/μm^2) show the decreasing of Raman bands intensity of yeast cells, while longer exposure resulted in the growth of some additional bands (above 1080, 1350 and 1580 (redistribution of the visible bands) cm^{-1}). Analyses of the chemical images – graphical fingerprint which represent the relative intensity of typical Raman bands – verify this conclusion (Fig. 6). Spectral fingerprint of the sample with relatively short duration only slightly different from initial one, while at longer exposure essential changes of fingerprint, has been observed. At the last case, the degradation of protein specific bands shows a stronger decrease in the number of exposure photons in respect to the lipids (1730 cm^{-1}). This implies that preferably the degradation of proteins is associated with thermal photodecomposition.

For the sample with irradiated time more than one minute simultaneously with decreasing of protein specific scattering (preferable within the Amide bands indicating the features of protein secondary

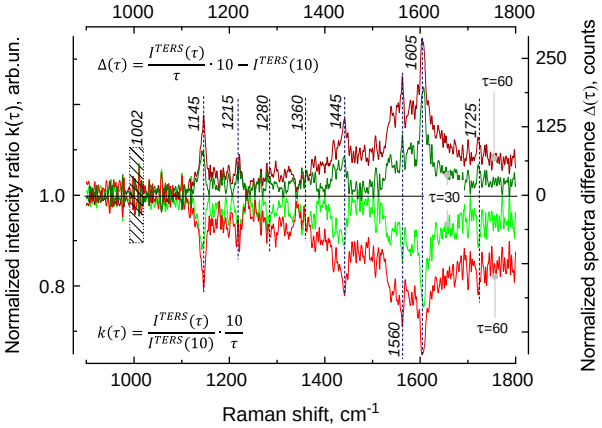

Fig. 4. Normalized intensity ratio $k(\tau)$ (bottom) and spectra difference $\Delta(\tau)$ (top) of μ-TERS spectra for acquisition time τ of 40 and 100 s scaled to the $\tau=10$ s. Shaded area at *c.a.* 1000 cm^{-1} shows that intensity of the Raman band specific for nonpolar phenylalanine amino acid (1004 cm^{-1}) do not fade essentially with increasing an acquisition time.

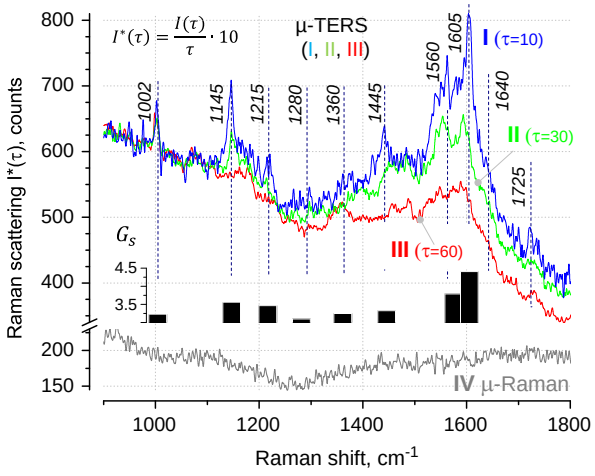

Fig. 3. Substrate corrected μ-Raman and μ-TERS spectra of single layer envelope of yeast cells (632.8 nm, 13 μW/μm^2 within the sample plane, acquisition time 10, 30 and 60 s). μ-TERS spectra (I (10 s), II (30 s), III (60 s)) have been scaled to the same acquisition time (10 s). Insert: experimentally observed band-specific enhancement factor G_s.

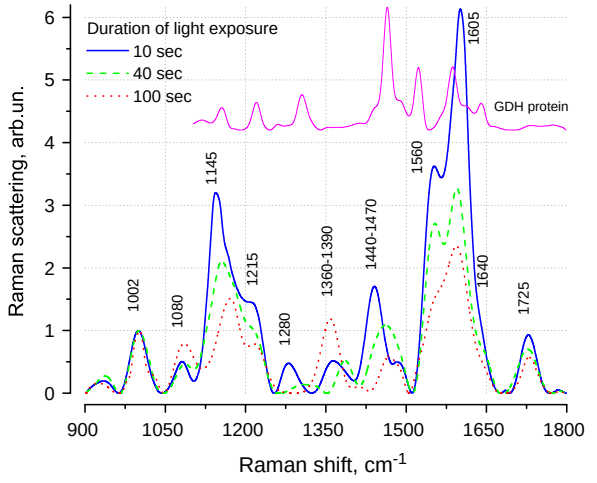

Fig. 5. Substrate and luminescence corrected (using wavelet and moving average filters for smoothing and a fourth order polynomial curves for multipoint baseline) μ-TERS spectra (presented in Fig. 3) of single layer envelope of yeast cells normalized to an intensity of a sharp band at 1004 cm^{-1} specific for the phenylalanine ring breathing vibrations. Inset: the spectra of single GDH protein (532 nm, 1 mW within the sample plane, acquisition time 120 s).

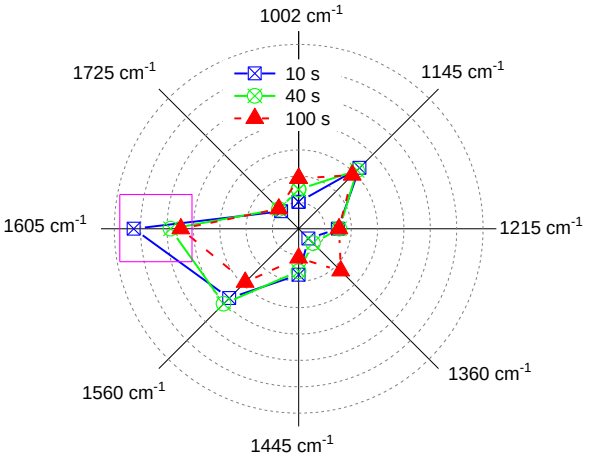

Fig. 6. Polar diagrams represented virtual fingerprint of the Raman spectra presented in Fig. 5 for different duration times.

structure) a relative increasing of the intensity in the regions at *c.a.* 1080, 1350 and 1580 cm^{-1} has been observed indicating the possible presence of amorphous carbon in this material. Indeed [56,57], the Raman spectra of disordered and amorphous carbons show several common features – the so-called D (disorder-induced peak) and *G* (graphite peak) bands around 1350 and 1600 cm^{-1} and an extra *T* peak which lie at around 1060 cm^{-1}. It is reasonable to note, that the same dried cell envelope samples on the surface of the Klarite® SERS substrates (data not shown) demonstrate immediate degradation and occurrence of carbon-specific bands at the same light intensity.

However, for the duration of laser light less than above 30 s there are no differences between the virtual chemical fingerprints observed (Fig. 5); so, the μ-TERS techniques can be efficiently used for adequate fingerprinting of the single layer of dried biological objects under relatively high level of laser illumination (13 μW/μm^2).

5. Discussion

The obtained results allow us to distinguish some issues which are essential for adequate characterization of biological samples under μ-TERS conditions, namely

- what are allowable limits for damage-free analysis of biological objects, in particular dried counterparts of single leaving cells;
- how to use potential for analysis of buried or subsurface structures for estimating the relative position of the scatterer in respect to the tip apex;
- what kind of the photo-destruction processes in biological material under μ-TERS conditions can be induced and
- how to control carbon contamination in transition.

Before the discussing the practical aspects of μ-TERS technique outlined above it is reasonable to stress that the Raman spectra of the cell envelope of the single living cells [31] and their dried extracted fractions in multilayers [54] or as the single-layer fragments differ from each other. Indeed, despite the similarity of the bands' positions the intensity distribution is specific for each type of sample. The first reason for that is difference in methodological approaches used for Raman spectra recording with reasonable level of signal to noise ratio. For example, in the case of single living cells the spectra represent averaged scattering across a whole cell [31] whilst the spectrum for multilayer dried structures are obtained under conditions of photo-induced luminescence self-quenching [54]. So, both the measurement approaches and sample preparation procedures have an impact on the final result. Indeed, biological structures are adaptive systems with elements optimized for operation under strictly defined conditions. Fragments of the cell wall located on the surface of living cells or on the glass surface are quite different in both structure and, probably, composition. Thus, direct comparison of the spectra of complex systems like cell envelope in such different environments as living cell and dried sample may lead to misrepresentation of the reality. An example is the significant difference in threshold of thermal decomposition of cellular envelope in the living cell and their dried counterparts on the glass substrate. To understand the reasons for these differences it is necessary to analyze the structure of the cell envelope of yeast.

The yeast envelope comprises the yeast cell wall (above 100 nm, up to 30% of the dry weight of the cell and up to 50% of the volume), periplasmic space (3–5 nm) and the plasma membrane (7–10 nm) [58]. The yeast cell wall is made mainly of helical glucans (35–55%, mainly a highly branched 1,3-β-glucan), structural protein – mannoproteins (30–50%), and some chitin (1.5–6%) [59]. So, it is reasonable to expect that Raman spectra will be a combination of spectra originated from the main fractions. Indeed, many weak peaks are well correlated with a highly branched 1,3-β-glucan and 1,6-β-glucan [60] and mannoproteins. The comparative analysis of the μ-TERS spectra of dried samples and single living cells [31] indicate an increased level of lipids in the first case (the ester peak at 1730 cm^{-1} [61]). This observation suggests that the internal side of yeast cell envelope with bilayer lipid membrane directed to the tip whereas the outer boundary is in touch with the substrate. The high level of protein content (1500–1600 cm^{-1}) within the area occupied by the evanescent wave is well correlated with proposed orientation of the cell envelope on the surface because of their natural arrangement within the periplasm [55]. These features allow us to confirm the directional and gradient character of μ-TERS technique, resulting in a higher sensitivity for the layers that are closer to the apex of the tip.

According to our previous results, the processes of photo-bleaching and thermal decomposition ("carbon contamination") observed for dried samples were absent in single living cells in the similar experimental conditions [31]. A significant decrease in the damage threshold of dried cell envelope is the result of the cell's ability to vary in composition and thickness depending on both external and internal factors. It is well known, that the cell wall may rapidly shrink indicating the combination of mechanical strength and elasticity of the construction [62]. The elasticity of the cell wall reflects the structure of the individual 1,3-β-glucan molecules, which have a flexible and helical shape, like a wire spring that can exist in various states of extension. Due to the presence of side-chains, 1,3-β-glucan molecules may only locally associate through hydrogen bonds, resulting in the formation of a continuous three-dimensional network. This network is highly elastic and considerably extended under normal osmotic conditions. So, it is reasonable to assume that after the cell destruction cell envelope tends to shrink – cell envelope may lose up to about 40–50% of initial surface [55,63] – and as a result become considerably denser than in living cell. In this case the possibility of heat-removing by water disappears, resulting in photo-destruction of the chromophore and its immediate environment as the thermalization of the electronic excitation at much lower light intensities.

μ-TERS technique as a version of Raman spectroscopy has a higher error protection because it allows to detect thermal degradation of the sample in transition by monitoring the emergence of specific Raman bands of disordered and amorphous carbons. In the case of dry samples initial decreasing of scattering of lipids and proteins followed by the degradation of proteins is associated with non-radiative complex formation or photo-destruction with some luminescence-free organic photoproduct [54]. This suggestion is in good agreement with the fact that, photo-destruction of plasma membrane of *S. cerevisiae* permeability barriers is important for yeast cell lethality [64]. The porphyrin-type compounds, naturally

located within lipid membrane and periplasm, are considered to be the most probable candidate for the role of the sensitizer in photodynamic damage of yeast plasma membrane and cell inactivation by visible light. The relatively stable intensity of the phenylalanine amino acid Raman band may be the result of the hydrophobic nature of the benzyl side chain phenylalanine located far away from the porphyrin chromophore. Moreover, the aromatic modes of the phenyl rings are well identified due to the higher Raman cross section of the aromatic rings while their absorption spectrum occupy the higher energy region in respect to other amino acids.

Taking into account the results of Raman spectroscopy for characterization of molecular photodamage in single yeast cell envelope we suggest practical excitation conditions effective for μ-TERS observation of dried biological samples without photodamage-related spectral distortion – the allowable limits (practical maximum duration time) without the photoproduct becoming visible is above 30 s at 13 $\mu W/\mu m^2$ for 632.8 nm excitation wavelength.

6. Concluding remark

μ-TERS is a well suited generation technique for local fingerprinting of single living cells or their dried substructures. This technique has a few advantages when applied to the study of biological samples, namely (i) it is rapid, (ii) it is non-invasive, (ii) no damage is induced if suitable laser wavelength and intensities are used, (iv) may be implemented in both water and air environments without special sample preparation procedures, (v) locally targeted physical transducer may be easily located at definite place; (vi) versatile, different functional structures may be identified by their vibrational fingerprint using the same physical transducers; and (vii) μ-TERS may be used for buried or sub-surface structures.

It is reasonable to note that proposed technique is the further development of Raman techniques based on single gold microshell tailored to sensitive probe [65], TERS with tip apex modified by large nanoparticle [66], a tapered optical fiber coated with Drude metals [67–69], or shell-isolated nanoparticles [70]. One of the most promising further developments of the discussed evanescent field driving Raman concept is a design of the plasmon enhanced light sources suitable for the time-resolved emission or scattering spectroscopy with up to attosecond level resolution [71].

Contrary to the classical TERS with sharp tips the mass production of reproducible μ-TERS tips can be easy realized by the routine microelectronic technologies that open the way to overcome the bottleneck in the wide application of the TERS technology. Commercial availability of the piezoelectric scanners, miniature lasers and integrated optical detectors, as well as the feasibility of μ-TERS technique with tips of micron size stimulate the development of simple and compact Raman spectrometers combined with SPP based optical scanners for wide applications in the near future. If true, this technique can help to design biologically correct but versatile measurement procedures for biological samples, and can be used for rapid, high throughput medical diagnostic, toxicological studies and testing of new pharmaceuticals.

Acknowledgments

The authors thank European Community Mobility Programme EMA2 (B.S.). This research was funded by the European Social Fund under the Global Grant measure.

References

[1] Y. Lin, R. Trouillon, G. Safina, A.G. Ewing, Anal. Chem. 83 (2011) 4369–4392.
[2] N.P. Ivleva, M. Wagner, H. Horn, R. Niessner, C. Haisch, Anal. Chem. 80 (2008) 8538–8544.
[3] K.D. Alexander, Z.D. Schultz, Anal. Chem. 84 (2012) 7408–7414.
[4] T. Ruckstuhl, C.M. Winterflood, S. Seeger, Anal. Chem. 83 (2011) 2345–2350.
[5] T. Ruckstuhl, D. Verdes, C.M. Winterflood, S. Seeger, Opt. Express 19 (2011) 6836–6844.
[6] D. Cialla, A. März, R. Bohme, F. Theil, K. Weber, M. Schmitt, J. Popp, Anal. Bioanal. Chem. 403 (2012) 27–54.
[7] J. Neng, M.H. Harpster, W.C. Wilson, P.A. Johnson, Biosens. Bioelectron. 41 (2013) 316–321.
[8] S. Berweger, M. Raschke, Anal. Bioanal. Chem. 396 (2009) 115–123.
[9] H.J. Lo, H.I. Hsiung, S. Chattopadhyay, H.C. Han, C.F. Chen, J.P. Leu, K.H. Chen, L. C. Chen, Biosens. Bioelectron. 26 (2011) 2413–2418.
[10] C. Budich, U. Neugebauer, J. Popp, V. Deckert, J. Microsc. 229 (2008) 533–539.
[11] K.M. Syamala, H. Abe, Y. Fujita, K. Tomimoto, V. Biju, M. Ishikawa, Y. Ozaki, T. Itoh, Langmuir 28 (2012) 8952–8958.
[12] A. Sujith, T. Itoh, H. Abe, K. Yoshida, M.S. Kiran, V. Biju, M. Ishikawa, Anal. Bioanal. Chem. 394 (2009) 1803–1809.
[13] D.N. Mehtani, N. Lee, R.D. Hartschuh, A. Kisliuk, M.D. Foster, A.P. Sokolov, J. F. Maguire, J. Raman Spectrosc. 36 (2005) 1068–1075.
[14] N. Anderson, A. Hartschuh, S. Cronin, L. Novotny, J. Am. Chem. Soc. 127 (2005) 2533–2537.
[15] T.A. Yano, P. Verma, Y. Saito, T. Ichimura, S. Kawata, Nat. Photonics 3 (2009) 473–477.
[16] Z.L. Zhang, L.i. Chen, S.X. Sheng, M.T. Sun, H.R. Zheng, K.Q. Chen, H.X. Xu, Front. Phys. 9 (2014) 17–24.
[17] Y. Kumamoto, A. Taguchi, N.I. Smith, S. Kawata, Biomed. Opt. Express 2 (2011) 927–936.
[18] M. Chaigneau, G. Picardi, R. Ossikovski, Surf. Sci. 604 (2010) 701–705.
[19] M. Sun, Z. Zhang, H. Zheng, H. Xu, Scientific Rep.2 (2012) 647.
[20] M.I. Stockman, Opt. Express 19 (2011) 22029–22106.
[21] S. Berweger, J.M. Atkin, R.L. Olmon, M.B. Raschke, J. Phys. Chem. Lett. 1 (2010) 3427–3432.
[22] M.I. Stockman, Phys. Rev. Lett. 93 (2004) 137404.
[23] S. Berweger, J.M. Atkin, R.L. Olmon, M.B. Raschke, J. Phys. Chem. Lett. 3 (2012) 945–952.
[24] B.A. Snopok, Theor. Exp. Chem. 48 (2012) 283–306.
[25] K.J. McKee, M.W. Meyer, E.A. Smith, Anal. Chem. 84 (2012) 9049–9055.
[26] X. Xuan, S. Xu, Y. Liu, H. Li, W. Xu, J.R. Lombardi, J. Phys. Chem. Lett. 3 (2012) 2773–2778.
[27] P.M. Boltovets, B.A. Snopok, Talanta 80 (2009) 466–472.
[28] B.A. Snopok, P.M. Boltovets, F.J. Rowell, Theor. Exp. Chem. 42 (2006) 217–223.
[29] P. Boltovets, S. Shinkaruk, C. Bennetau-Pelissero, B. Bennetau, B. Snopok, Talanta 84 (2011) 867–873.
[30] P.M. Boltovets, O.M. Polischuk, O.G. Kovalenko, B.A. Snopok, Analyst 138 (2013) 480–486.
[31] D. Naumenko, V. Snitka, E. Serviene, I. Bruzaite, B. Snopok, Analyst 138 (2013) 5371–5383.
[32] W. Zhang, T. Schmid, B.S. Yeo, R.J. Zenobi, Phys. Chem. C 112 (2008) 2104–2108.
[33] K. Hasegawa, J.U. Noeckel, M. Deutsch, Phys. Rev. A 75 (2007) 063816–063819.
[34] D.R. Mason, D.K. Gramotnev, K.S. Kim, Opt. Express 20 (2012) 12866–12876.
[35] K. Kneipp, M. Moskovits, H. Kneipp (Eds.), Physics and Applications. Series: Topics in Applied Physics, vol. 103, 2006.
[36] W. Zhu, I.D. Rukhlenko, M. Premaratne, Photonics J. 4 (2012) 741–747.
[37] H.M. Barlow, A.L. Cullen, Proc. IEE 100 (1953) 329–347.
[38] M. Lucas, E. Riedo, Rev. Sci. Instrum. 83 (2012) 061101.
[39] L.S. Jung, C.T. Campbell, T.M. Chinowsky, et al., Langmuir 14 (1998) 5636–5648.
[40] Yu.V. Krylenko, Yu.A. Michailov, A.S. Orechov, G.S. Sklizkov, Preprint of the Lebedev Physical Institute of the Russian Academy of Sciences, N4, 2010, 1–47.
[41] E.A. Bibikova, N.D. Kundikova, L.F. Rogacheva, Izv. Cheliabinskogo Nauchnogo Cent. 3 (2006) 1–5.
[42] K. Youngworth, T. Brown, Opt. Express 7 (2000) 77–87.
[43] Y. Saito, M. Kobayashi, D. Hiraga, K. Fujita, S. Kawano, N.I. Smith, Y. Inouye, S. Kawata, J. Raman Spectrosc. 39 (2008) 1643–1648.
[44] D. Kurouski, T. Postiglione, T. Deckert-Gaudig, V. Deckert, I.K. Lednev, Analyst 138 (2013) 1665.
[45] E. Servienė, S. Pilevičienė, V. Časaitė, Rom. Biotechnol. Lett. 15 (2010) 5773–5780.
[46] S. Pileviciene, A. Lebionka, E. Serviene, Proc. Natl. Acad. Sci. Belarus 4 (2010) 209–212.
[47] L.A. Reisner, A. Cao, A.K. Pandya, Chemom. Intell. Lab. Syst. 105 (2011) 83–90.
[48] A. Cao, A.K. Pandya, G.K. Serhatkulu, R.E. Weber, H. Dai, J.S. Thakur, V.M. Naik, R. Naik, G.W. Auner, R. Rabah, D.C. Freeman, J. Raman Spectrosc. 38 (2007) 1199–1205.
[49] B.A. Snopok, I.V. Kruglenko, Sens. Actuators B: Chem. 106 (2005) 101–113.
[50] B.A. Snopok, I.V. Kruglenko, Thin Solid Films 418 (2002) 21–41.
[51] V. Dupres, Y.F. Dufrêne, J.J. Heinisch, ACS Nano 28 (2010) 5498–5504.
[52] P. Roesch, M. Harz, K.D. Peschke, O. Ronneberger, H. Burkhardt, J. Popp, Biopolymers 82 (2006) 312–316.
[53] J. Chan, S. Fore, S. Wachsmann-Hogiu, T. Huser, Laser Photonics Rev. 2 (2008) 325–349.
[54] D. Naumenko, B. Snopok, E. Serviene, I. Bruzaite, V. Snitka, Theor. Exp. Chem. 49 (2013) 228–234.
[55] F.S. Klis, A. Boorsma, P.W.J. De Groot, Yeast 23 (2006) 185–202.
[56] A.C. Ferrari, J. Robertson, Phys. Rev. B 64 (2001) (075414-13).
[57] G.E. Remneva, V.V. Uglov, V.I. Shymanski, P. Konarski, M.P. Samtsov, S. K. Pavlov, N.M. Lapchuk, Vacuum 89 (2013) 118e121.
[58] P.N. Lipke, R. Ovalle, J. Bacteriol. 180 (1998) 3735–3740.

[59] E. Cabib, D.H. Roh, M. Schmidt, L.B. Crotti, A. Varma, J. Biol. Chem. 276 (2001) 19679–19682.
[60] M. Novak, A. Synytsya, O. Gedeon, P. Slepička, V. Prochazka, A. Synytsya, J. Blahovec, A. Hejlova, J. Copikova, Carbohydr. Polym. 87 (2012) 2496–2504.
[61] R. Bohme, D. Cialla, M. Richter, P. Rosch, J. Popp, V. Deckert, J. Biophotonics 3 (2010) 455–461.
[62] N.E. Ziołkowska, R. Christiano, T.C. Walther, Trends Cell Biol. 22 (2012) 151–158.
[63] F. Ricchelli, J. Photochem. Photobiol. B 29 (1995) 109–118.
[64] G.Ya. Fraikin, M.G. Strakhovskaya, A.B. Rubin, J. Photochem. Photobiol. B: Biol. 34 (1996) 129–135.
[65] L. Piao, S. Park, H.B. Lee, K. Kim, J. Kim, T.D. Chung, Anal. Chem. 82 (2010) 447–451.
[66] Z.D. Schultz, S.J. Stranick, I.W. Levin, Anal. Chem. 81 (2009) 9657–9663.
[67] D.L. Stokes, Z. Chi, T. Vo-Dinh, Appl. Spectrosc. 58 (2004) 292–298.
[68] A. Passian, R.H. Ritchie, A.L. Lereu, T. Thundat, T.L. Ferrell, Phys. Rev. B 71 (2005) 115425.
[69] A.L. Lereu, A. Passian, P. Dumas, Int. J. Nanotechnol. 9 (2012) 488–501.
[70] J.F. Li, Y.F. Huang, Y. Ding, Z.L. Yang, S.B. Li, X.S. Zhou, F.R. Fan, W. Zhang, Z. Y. Zhou, D.Y. Wu, B. Ren, Z.L. Wang, Z.Q. Tian, Nature 464 (2010) 392–395.
[71] M. Lupetti, M.F. Kling, A. Scrinzi, Plasmon enhanced attosecond extreme ultraviolet source, Phys. Rev. Lett. 110 (2013) 223903.